Energies **2013**, *6*, 3706-3733; doi:10.3390/en6083706

OPEN ACCESS

energies

ISSN 1996-1073

www.mdpi.com/journal/energies

Article

Exploring the Potential for Increased Production from the Wave Energy Converter Lifesaver by Reactive Control

Jonas Sjolte [1,2,*], Christian McLisky Sandvik [2], Elisabetta Tedeschi [3] and Marta Molinas [2]

[1] Fred. Olsen, Fred. Olsens Gate 2, N0152 Oslo, Norway

[2] Department of Electric Power Engineering, Norwegian University of Science and Technology, O.S. Bragstads plass 2E, N-7034 Trondheim, Norway; E-Mails: mcliskysandvik@gmail.com (C.M.S.); marta.molinas@ntnu.no (M.M.)

[3] SINTEF Energy Research, Postbox 4761 Sluppen, Trondheim 7465, Norway; E-Mail: tedeschi@ieee.org

* Author to whom correspondence should be addressed; E-Mail: jonas.sjolte@ntnu.no; Tel.: +47-223-411-45; Fax.: +47-223-424-15.

Received: 5 March 2013; in revised form: 22 May 2013 / Accepted: 23 June 2013 / Published: 25 July 2013

Abstract: Fred Olsen is currently testing their latest wave energy converter (WEC), Lifesaver, outside of Falmouth Bay in England, preparing it for commercial operation at the Wavehub test site. Previous studies, mostly focusing on hydrodynamics and peak to average power reduction, have shown that this device has potential for increased power extraction using reactive control. This article extends those analyses, adding a detailed model of the all-electric power take-off (PTO) system, consisting of a permanent magnet synchronous generator, inverter and DC-link. Time domain simulations are performed to evaluate the PTO capabilities of the modeled WEC. However, when tuned towards reactive control, the generator losses become large, giving a very low overall system efficiency. Optimal control with respect to electrical output power is found to occur with low added mass, and when compared to pure passive loading, a 1% increase in annual energy production is estimated. The main factor reducing the effect of reactive control is found to be the minimum load-force constraint of the device. These results suggest that the Lifesaver has limited potential for increased production by reactive control. This analysis is nevertheless valuable, as it demonstrates how a wave-to-wire model can be used for investigation of PTO potential, annual energy production estimations and evaluations of different control techniques for a given WEC device.

Keywords: wave energy; reactive control; lifesaver; wave-to-wire model; power take-off; point absorber

1. Introduction

With increasing oil prices and the consequent focus on shifting the world energy-dependency towards renewable resources, wave energy has regained increased attention. It is estimated that when today's technology is fully matured, around 140–750 TWh will be commercially exploitable annually [1]. If all potential technology is realized, this number can be greatly increased, with some scenarios as large as 2000 TWh, corresponding to approximately 10% of the global electricity consumption in 2008 [2]. One of such technologies, developed by the Fred Olsen Wave Energy Project *Bolt2Wavehub*, named *Lifesaver*, was deployed in early 2012 as a stand-alone system at Falmouth Bay, England. The next step is to make it commercially ready and launch it at Wavehub [3].

The control method used on the *wave energy converter* (WEC) greatly affects the output power, and the selection and optimization of control method for the Lifesaver system will be the focus of this work. The theoretical control method for optimal power extraction is well-established, thanks to the pioneering work of Falnes [4,5]. He shows that the optimal power extraction occurs when the system is controlled with a 90° phase-shift between wave motion and absorber motion, a method referred to as *complex-conjugate* control or *reactive* control. Due to the irregular nature of ocean waves, such a production mode can only be maintained by active control of the power extraction system and requires the real-time phase and frequency information of the incoming waves. Falnes and his team have suggested practical solutions and optimization methods toward this [6,7], but attaining accurate real-time wave information has proven difficult, and several methods of sub-optimal control have been suggested to make up for this [8].

During the current deployment, the performance of the Lifesaver *power take-off* (PTO) and the impact of the control strategy on the PTO is of great interest. The design process of Lifesaver has shown that the production machines are by far the most expensive component in the system and that the absorber hull is relatively cheap in comparison. This forces a major shift in control strategy from the traditional control method that focuses on maximizing the absorber output. Instead, Lifesaver is optimized towards maximizing the PTO utilization, which leads to a control method based on damping, where the production force is proportional to the absorber speed. In this control mode, the production force are in phase with the production speed and are referred to as *active forces*, as opposed to a complex-conjugate control that requires *reactive forces*, which reduce the PTO utilization [9]. The damping control selected at Lifesaver also avoids the need of real-time wave information and allows for a simple and robust time-invariant control.

However, initial investigations indicate that Lifesaver might have potential for increased power extraction with reactive control during calmer sea states [10], by utilizing free production capacity. These investigations have so far focused on the hydrodynamic model of the WEC and on optimizing average power while reducing the peak-to-average power ratio, while less attention has been paid to the

physical limitations of the generator, switchgear and the rest of the PTO system. The purpose of this study is therefore to develop a full wave-to-wire model of Lifesaver with an all-electric PTO system. The model is used to evaluate the effect of different control strategies on the PTO capabilities under different sea state conditions. Such a study is interesting, since the power extraction capabilities of a WEC device will be strongly dependent on the impact of the control strategy implemented. Depending on the WEC device, parameters and physical constraints of the PTO system, a control strategy with a reactive component can potentially increase the energy production and, therefore, be an important factor for the commercial exploitation possibilities of the WEC concept.

1.1. Description of the Investigated System

Lifesaver consists of five point absorbers with individual PTO systems connected together on a toroid shaped device. The PTOs are all-electric systems sharing a common DC-Link and uses an electric energy storage to power the generators and to maintain continuous rope tension. This means that each generator will have to operate in motoring mode and wind in the rope on downward movement of the device, meaning that some energy will have to be supplied to the system in this part of the oscillatory cycle. Having the PTOs on a common platform gives obvious economical advantages and allows, among other things, to utilize the pitching motion created on the device by the sea. Lifesaver is pictured on site outside Falmouth, England, in Figure 1. Figure 2 illustrates the function of the PTO and WEC system.

Figure 1. *Lifesaver* on site outside Falmouth, England.

For the purpose of this study, a simplified representation of the system is defined, which consists of a single point absorber coupled to an all-electric PTO system (generator and inverter including the DC-link). This module is defined as the basis for the design of the wave-to-wire model in this paper. To model the full Lifesaver system, several modules are employed in parallel to simulate multiple PTOs. Lifesaver is prepared for operation with five PTOs, which is the basis for this work, but currently only operates with three PTOs.

Figure 2. Lifesaver power take-off (PTO) function.

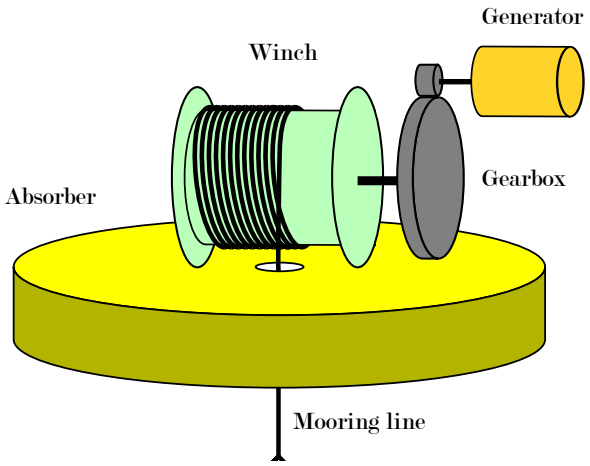

2. Hydrodynamic Model

The hydrodynamic model of Lifesaver has the following input:

- Wave elevation time-series;
- Load force, F_L, given by the load force parameters, damping, B_L, and added mass, M_L.

The output of the model is the velocity, $\dot{\eta}$, and acceleration, $\ddot{\eta}$, of the device. In this work, the hydrodynamic model is realized as a one *degrees of freedom* (DOF) model and only models heaving motion. In simulation work that demands high accuracy, we use a more complex three-DOF model that takes into account heaving, surging and pitching motion. However, as this work focus on the electrical performance, with a relative comparison of the output result, we believe that the simplified one-DOF model is sufficient for this work.

2.1. Generation of Wave Elevation Time Series

A common way to model the sea is by using an energy spectrum. There are various mathematical models that are used for defining such spectra, and the most widely known is the two-parameter Bretschneider spectrum [11]. The preferred analytical form of the frequency spectrum, $S(\omega)$, is given in Equation (1).

$$S_{(\omega)} = \frac{5}{16} H_s^2 \frac{\omega_0^4}{\omega^5} e^{-\frac{5\omega_0^4}{4\omega^4}} \tag{1}$$

here, H_s is the significant height of the sea state; and ω_0 is the peak frequency. Figure 3 shows the Bretschneider spectra for different values of the peak frequency. The time-domain wave elevation of the real sea waves can be regarded as the super-position of different frequency sinusoidal waves. Thus, the energy spectrum can be used to represent the sea by summing a large, but finite, number of different frequency components of infinitesimal height and random phase. The elevation due to each such wave components can be expressed by Equation (2) [12].

$$\zeta_n(t) = \sqrt{2S(\omega_n)d\omega}\sin(\omega_n t + \phi_n) \tag{2}$$

here, ϕ_n is the randomly generated offset angle for each wave component; n. By summing these waves, the wave elevation time-series is created as described by Equation (3). A typical output time-series is plotted in Figure 4.

Figure 3. Bretschneider spectra for different values of the peak period, $T_p[s]$.

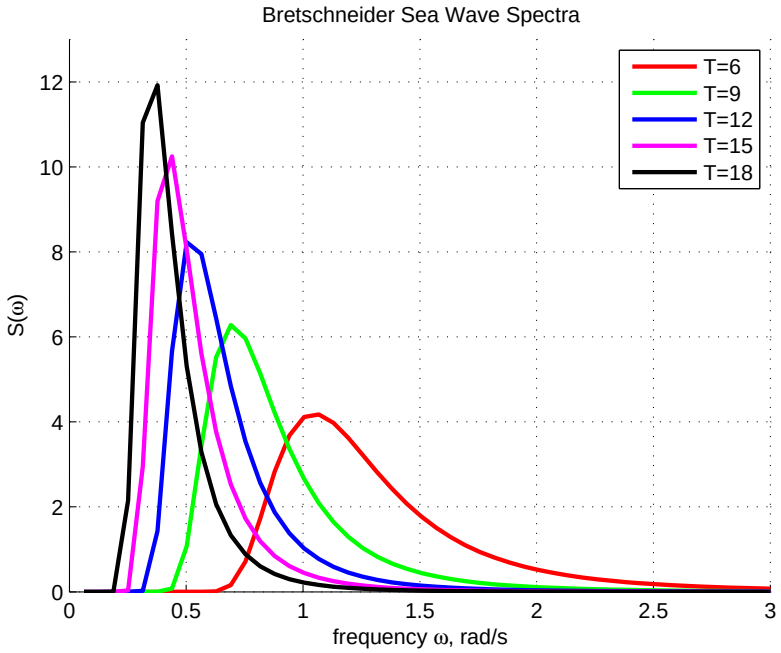

$$\zeta(t) = \sum_{n=1}^{N} \sqrt{2S(\omega_n)d\omega}\sin\left(\omega_n t + \phi_n\right) \tag{3}$$

Figure 4. Time-series of a Bretschneider spectrum, $H_s = 7m$ and $T_p = 11s$.

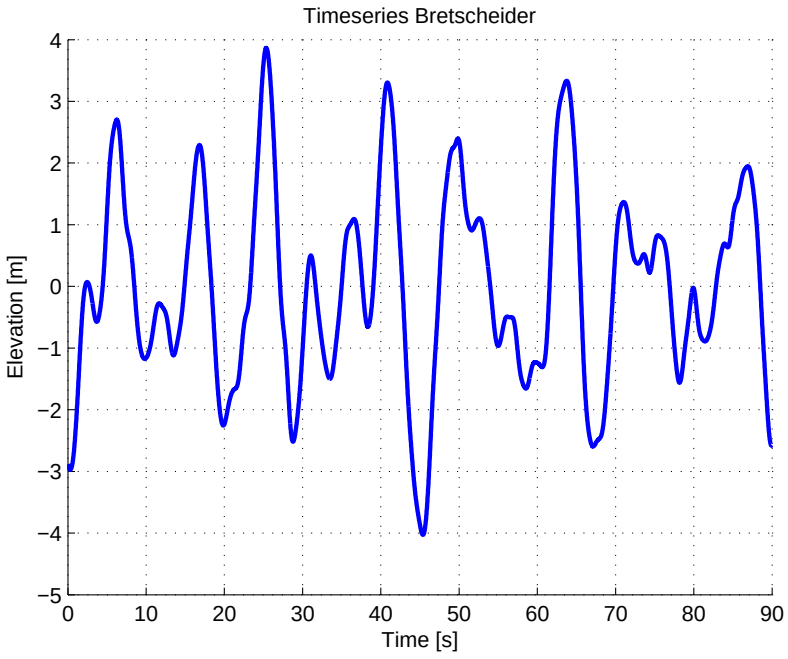

2.2. Forces Acting on the WEC System

$$M\ddot{\eta} = f_e(t) + f_s(t) + f_r(t) + f_m(t) \tag{4}$$

Equation (4) calculates the force balance for a buoy excited by an incoming wave, where η is the device position with respect to the equilibrium position; and M is the equivalent mass of the WEC system, consisting of the mass of the WEC and the inertia of the power take off system [13]. f_e is the excitation force; f_r is the radiation force; f_m is the machinery force, or the force related to the power take off system; and f_s represents the hydrostatic force. In this model, the mooring forces, viscous forces and environmental forces are disregarded.

2.2.1. Hydrostatic Force

The hydrostatic force is the resultant force of gravitational forces and forces acting on the buoy due to displaced water and is calculated with Equation (5), where k_s represents the hydrostatic stiffness. Commonly, the stiffness is considered a constant value, and thus, the force is proportional to device displacement, η [8].

$$f_s = k_s\eta \tag{5}$$

2.2.2. Radiation Force

An oscillating device will create a diffraction wave, and the force acting on the device due to this wave is referred to as the radiation force. In the frequency domain, it is typically expressed by Equation (6), where m_r is the added mass of the water oscillating with the device and R_r is the radiation resistance. As these parameters are frequency dependent, the time domain expression of the radiation resistance can be described by Equation (7) [14].

$$\hat{F}_R(\omega) = m_r(\omega)\ddot{\eta} + R_r(\omega)\dot{\eta} \tag{6}$$

$$F_r(t) = m_r(\infty)\ddot{\eta} + \int_0^t k(t-\tau)\dot{\eta}(\tau)d\tau \tag{7}$$

In the first term of the right-hand side of this expression, $m_r(\infty)$ is the added mass at infinite frequency. The second term is a convolution integral, where the convolution kernel, k, can be considered the radiation force impulse response. As discussed by Hals [8], a good approximation is to replace this convolution term by the state-space equivalent represented by Equations (8) and (9).

$$F_r(t) = \mathbf{C}_k\mathbf{z}(t) + \mathbf{D}_k\dot{\eta}(t) \tag{8}$$

$$\dot{\mathbf{z}}(t) = \mathbf{A}_k\mathbf{z}(t) + \mathbf{B}_k\dot{\eta}(t) \tag{9}$$

Taghipour, Perez and Moan show in [15] how the *Realization Theory* can be used in order to identify the state-space parameters, $\mathbf{A}_k$, $\mathbf{B}_k$, $\mathbf{C}_k$ and $\mathbf{D}_k$. By identifying the discrete radiation impulse response

through inverse Fourier transform of $k(\omega)$, as shown in Equation (10), a state-space system with a corresponding impulse response is generated.

$$k(\omega) = i\omega\{m_r(\omega) - m_r(\infty)\delta(\omega)\} + R_r(\omega) \tag{10}$$

The values for radiation resistance and the added mass of Lifesaver in the frequency domain are known and supplied by Fred Olsen for a range of frequencies. This impulse response fitting is realized using the Matlab Robust Toolbox function *imp2ss*, which is based on the Hankel Singular value decomposition proposed by Kung [16]. Using this, a state-space system is generated and a good representation of the radiation force is obtained. A more thorough explanation of how the radiation force is modeled for Lifesaver is given in [10].

2.2.3. Excitation Force

The force that the incident wave exerts on the WEC body is called the excitation force. It is given by the elevation of the sea, ζ, and the excitation force coefficient, $H_{F\zeta}$, as defined in Equation (11).

$$F_{e,c}(\omega) = H_{F,\zeta}(\omega)\zeta(\omega) \tag{11}$$

this coefficient is known and supplied by Fred Olsen for a range of frequencies. In a similar way, as for the radiation force, the time domain expression of the excitation force becomes a convolution term [8], as described by Equation (12).

$$F_{e,c}(t) = \int_0^t h_{F\zeta}(t - \tau_c)\zeta(\tau)d\tau \tag{12}$$

A state space representation of the convolution term is then found in the same manner as outlined for the radiation force; by impulse response fitting with the discrete excitation force impulse response extracted from the excitation force coefficients.

2.2.4. Load Force

The load force, F_L, or machinery force, is the force applied to the system by the PTO. The magnitude of this force, and how this force is applied, greatly influences the power extraction capabilities of the WEC. Typically, the load force is represented by one component proportional to the device velocity and a second component proportional to the device acceleration, as stated by Equation (13). B_L is considered the machinery damping; while M_L is the machinery added mass. Input into the wave-to-wire model is therefore either the load force or the load force parameters.

$$F_L = B_L\dot{\eta} + M_L\ddot{\eta} \tag{13}$$

3. Electric Power Take-off System

The Lifesaver PTO system, which is the basis for the model developed in this article, is all-electric. The stand-alone system, currently deployed outside the coast of England, consists of the following components:

- Permanent Magnet Synchronous Machine;
- Inverter/Rectifiers;
- Ultra-capacitor Bank;
- DC-link Charger;
- Battery Charger;
- Brake Charger and Dump Resistor.

In Lifesaver, all the PTO rectifiers are coupled in a common DC-link, as illustrated in Figure 5. The point absorber with PMSMand an inverter/rectifier is considered a complete system, which only needs to connect to a DC-link to operate. The scope of this section is to model one such module and to consider the DC-link as a constant voltage of 600 V. The electric system considered for the model is shown in Figure 6. The main specifications of the PTO, as defined by Fred Olsen, are given in Table 1.

Figure 5. Current topology of the stand-alone system for Lifesaver.

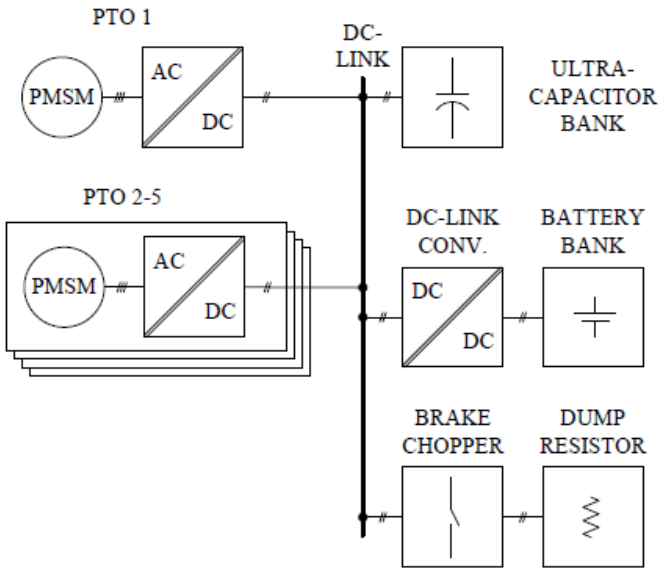

Figure 6. Schematic representation of the all-electric PTO system.

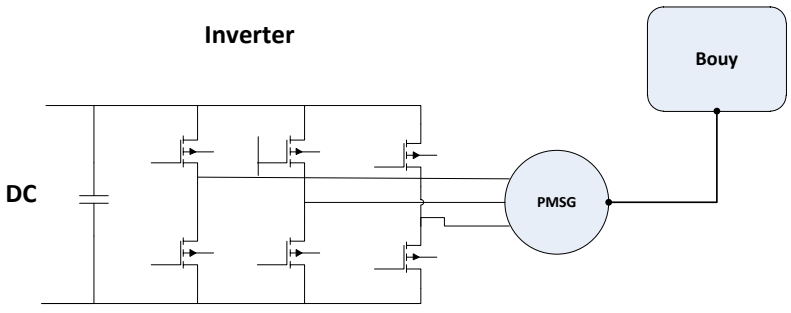

Table 1. Lifesaver PTO characteristics.

Property	Value	Unit
Generator nominal speed	400	rpm
Generator maximum torque	3700	Nm
DC-bus voltage	600	V
Angular to linear gear ratio	38.5	1/m
PTO maximum force	100	kN
PTO minimum force	10	kN
PTO nominal speed	1.1	m/s

3.1. PWM Converter Modeling

The PWMconverter is modeled with a time constant equal to unity in the comparably slow wave energy system. This implies that the voltage applied by the converter is considered to follow the reference voltage perfectly and instantly. This approach has the following advantages:

- Simulation time is significantly reduced. Even for low switching frequencies in the converter bridge, the simulation time becomes tenfold times longer than with the unity block solution;
- No filter is needed in the system in order to evaluate voltage measurements, as the harmonic distortion due to the high frequency switching is not present.

For the simulations that are being performed in this article, there are two important attributes to consider for the PWM converter. One is the maximum value of the voltage, which is set by the constant value of the DC-bus, and the other is the losses that occur in the converter. The first condition is handled by direct saturation of the voltage in the current controller and by advanced field-weakening control, as explained later. The losses are more difficult to evaluate, since not enough data is available of the converter used in the Lifesaver system. However, the inverter efficiency is included in the efficiency model provided in Section 3.3, so that a complete figure for the mechanical to electrical conversion efficiency is produced. The inverter losses are small compared to the generator and contributes with 3%–10% of the total losses.

3.2. Modeling and Control of the Permanent Magnet Synchronous Generator

In this model of the Lifesaver PTO, the generator is considered a 28 pole surface-mounted PMSM. The generator characteristics used for the model are given in Table 2.

For given voltages, u_q and u_d, on the generator terminals, the current equations for the PMSM are commonly expressed as stated by Equations (14) and (15) [17].

$$\frac{di_d}{dt} = -\frac{R_S}{L} i_d + \omega_e i_q + \frac{1}{L} u_d \tag{14}$$

$$\frac{di_q}{dt} = -\frac{R_S}{L} i_q - \omega_e \left(i_d + \frac{\Psi_{PM}}{L} \right) + \frac{1}{L} u_q \tag{15}$$

here, ω_e is the electric angular frequency of the generator; i_d and i_q are the d- and q-axis current; Ψ_{PM} is the rotor permanent magnet flux; while R_s and L are the stator resistance and inductance, as defined in Table 2. For a surface mounted PMSM, the inductance in the d- and q-axis can be considered equal.

Table 2. Generator characteristics.

Property	Value	Unit
Rated Power, P_n	83.7	kW
Rated Voltage, V_n	400	V
Number of poles, n_p	28	
Torque constant, k_T	10.8	Nm/A
Winding resistance, R_s	0.038	Ω
Inductance, L	1.4	mH
Inertia, J_{gen}	1.31	kgm^2
Permanent magnet flux,Ψ_{PM}	0.257	Wb

3.2.1. Current Control

As is known from d-q reference frame analysis [17], there is a cross coupling between the q-axis and the d-axis in Equations (14) and (15). This can be avoided by feed-forward technique, defining a reference voltage, $v_d = u_d + \omega_e L i_q$ and $v_q = u_q - \omega_e L i_d - e_q$. This gives two independent first-order equations in the d-q frame, as given by Equations (16) and (17). The transfer functions from current, i; to voltage, v, can thus be written as stated by Equation (18).

$$v_d = R_s i_d + L_s \frac{di_d}{dt} \tag{16}$$

$$v_q = R_s i_q + L_s \frac{di_q}{dt} \tag{17}$$

$$\frac{i(s)}{u(s)} = \frac{\frac{1}{R_s}}{1 + \frac{L_s}{R_s} s} \tag{18}$$

These current loops are controlled using PIregulators. Figure 7 shows the block diagram with the PI-controller, PWM and converter bridge included. As discussed earlier, the transfer block of the PWM and converter bridge is set to be unity.

Figure 7. Block diagram of current control loop. Notably, the PWM + converter block is represented by a unity gain.

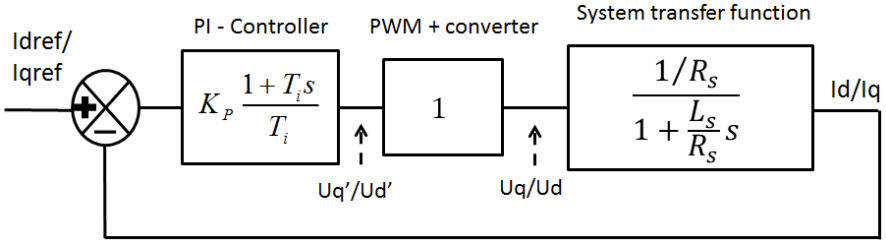

The parameters of these PI regulators are tuned according to the modulus optimum [18], canceling out the electrical time constant, $T_i = \frac{L_s}{R_s}$. This results in the open-loop transfer function expressed in Equation (19). Determination of gain, K_p, is done through evaluating the term for the closed loop transfer function. As it is desirable to have a closed loop transfer function gain equal to unity, a value for K_p can be approximated.

$$G_{OL} = K_p \frac{1 + T_i s}{T_i s} \frac{\frac{1}{R_s}}{1 + \frac{L_s}{R_s} s} = K_p \frac{\frac{1}{R_s}}{\frac{L_s}{R_s} s} = K_p \frac{1}{L_s s} \tag{19}$$

$$M(\omega) = \frac{G_{OL}}{1 + G_{OL}} = \frac{K_p}{L_s j\omega + K_p} = 1 \tag{20}$$

To obtain unity closed-loop gain, $K_p >> L_s\omega$, as shown in Equation (20). As the value for $L_s = 1.4$ mH and $\omega_{e,max} < n_{max} \frac{2\pi}{60} n_{pp} \approx 5,000$, it is considered that $K_p = 25$ is sufficiently large for all operation areas. In Figure 8, the current control with de-coupling and PI controllers is shown implemented in the Simulink block, named *current control*.

Figure 8. Current control implemented in Simulink.

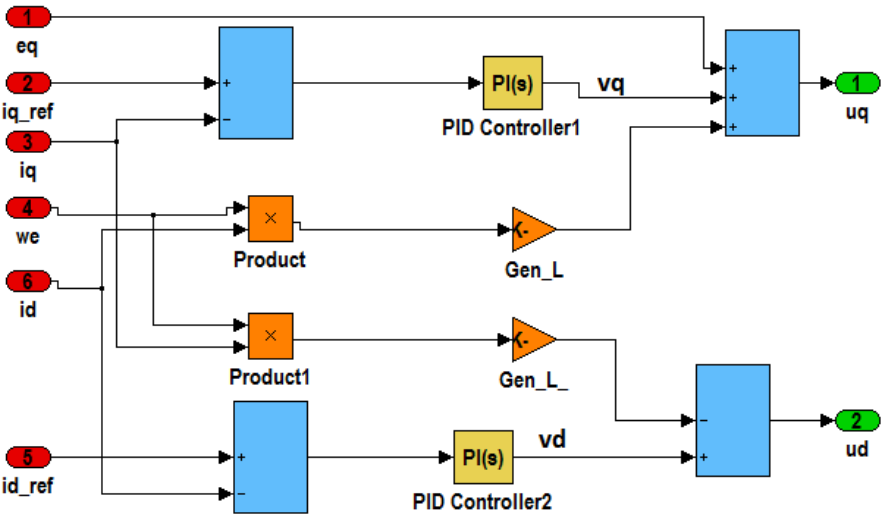

3.2.2. Torque Control

In order to make sure that the limitations of the electric PTOs are not exceeded, torque control is required. For low-speed operation, this is realized by maintaining a constant damping, B_L, and added mass, M_L. However, control is required to saturate the load-force at its maximum value, as well as to implement the field weakening control reference current-values. Initially, the torque control method over the entire range of operation speeds is designed to function as described in Figure 9. Here, I_{min} refers to the minimum torque constraint to keep tension in the rope.

The input into the torque-control flowchart in Figure 9 is the i_q reference current and the generator speed, ω_e. The reference current is obtained based on the reference torque from Equation (21). The reference torque is calculated from the mechanical model of the wave energy converter in Equation (22),

where ρ_g is the total gear ratio, including the linear-to-rotational radius, thus having the unit, $[\frac{1}{m}]$. The generator speed is also calculated from the mechanical model and is given by Equation (23).

$$i_{q,ref} = \frac{T_{e,ref}}{\frac{3}{2} n_p \Psi_{PM}} \tag{21}$$

$$T_{e,ref} = \frac{1}{\rho_g} (B\dot{\eta} + M_L \ddot{\eta}) \tag{22}$$

$$\omega_e = n_p \rho_g \dot{\eta} \tag{23}$$

Figure 9. Flowchart representing the idea behind the determination of current reference for the torque control.

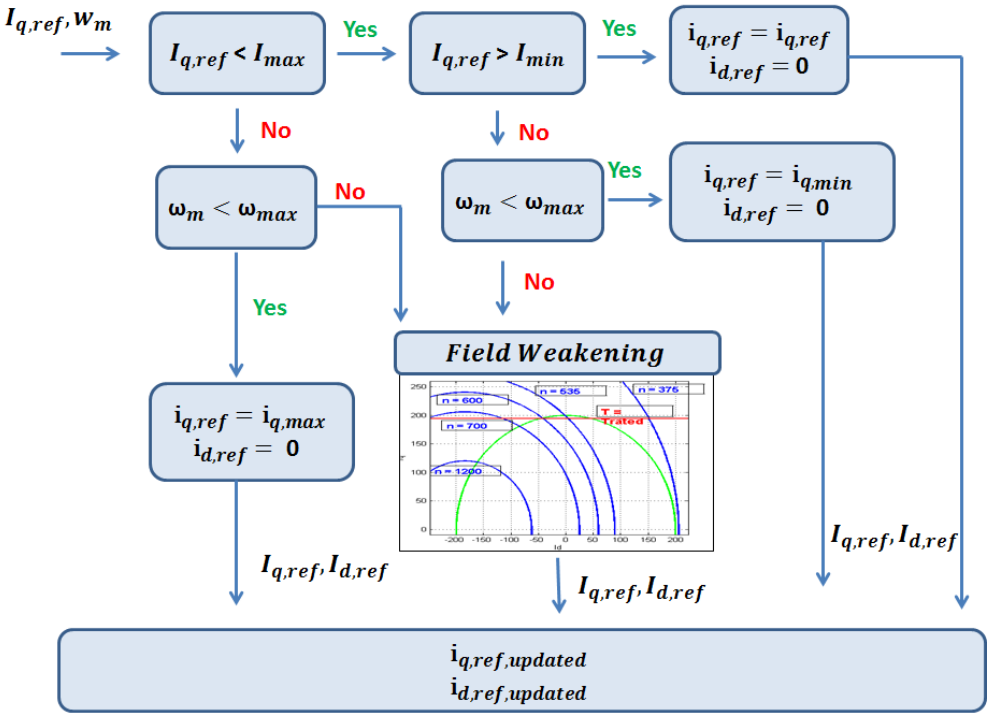

The speed at which field weakening begins, $\omega_{max} = \omega_{fw}$, can be expressed by the generator characteristics, as seen in Equation (24). The method used for determining the field weakening reference d- and q-axis currents is based on the robust field weakening control strategy described by Pan and Liaw [19].

$$\omega_{fw} = \frac{-2R_s I_{max} \Psi_{PM} + \sqrt{(2R_s I_{max} \Psi_{PM})^2 - 4(\Psi_{PM}^2 + L I_{max}^2)(R_s^2 I_{max}^2 - V_{max}^2)}}{2(\Psi_{PM}^2 + L^2 I_{max}^2)} \tag{24}$$

3.3. Generator Efficiency

As the detailed properties of the generator and converter are not known, it is not possible to make an accurate model of the system losses based on theoretical analysis. However, from the manufacturer of the generator and converter module, the efficiency at a number of operating points have been provided to Fred Olsen. This has been used to develop a polynomial expression for the combined generator and

converter losses as a function of generator torque, T_e; and speed, ω_e, as given by Equation (25). Due to a confidentiality agreement with the manufacturer, the actual figures cannot be disclosed. However, the resulting efficiency map plotted in Figure 10 gives a good understanding of the system performance.

$$P_{loss} = a_1 T_e^4 + a_2 T_e^2 + a_3|\omega_e| + a_4\omega_e^2 + a_5|\omega_e||T_e| + a_6|\omega_e|T_e^2 \quad (25)$$

Figure 10. Generator and converter efficiency map.

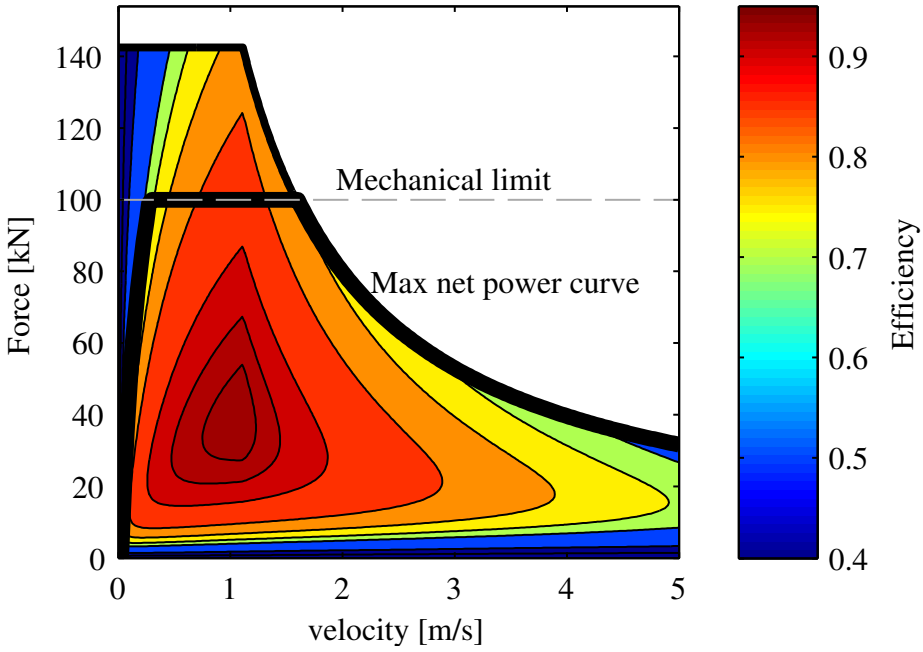

4. Wave-to-Wire Modeling

The complete wave-to-wire Simulink model of the WEC system of Lifesaver is shown in Figure 11. Previous investigations [10] show a large increase in average generated power when complex conjugate control is applied to the Lifesaver buoy. To further investigate this potential, full wave-to-wire simulations will be performed, where the physical limitations and efficiency of the all-electric PTO system are also included. When the control is being referred to as *complex conjugate*, it is meant that the load parameters are being tuned according to complex conjugate control equations [9] in the non-saturated mode of operation.

4.1. Simulation Results for a Passive Loaded System

The system is simulated for a low wave state with $H_s = 0.5\,m$ and $T_p = 6.5\,s$. The load coefficient is calculated as explained in [10] and results in damping, $B_L = 90$ kNs/m. In Figures 12 and 13, the input wave elevation and the corresponding generator speed is plotted. Notably, the generator speed is well below the torque saturation speed for the entire simulation time. The d-axis current, q-axis current and generator torque are shown in Figure 14, and in accordance with the generator speed plot, these plots show that torque saturation does not occur for this simulation. The constant zero d-axis current

also indicates that field weakening does not occur. The mechanical extracted power, generator losses and output electrical power is plotted in Figures 15 and 16.

Figure 11. Simulink wave-to-wire model of the wave energy converter (WEC), Lifesaver.

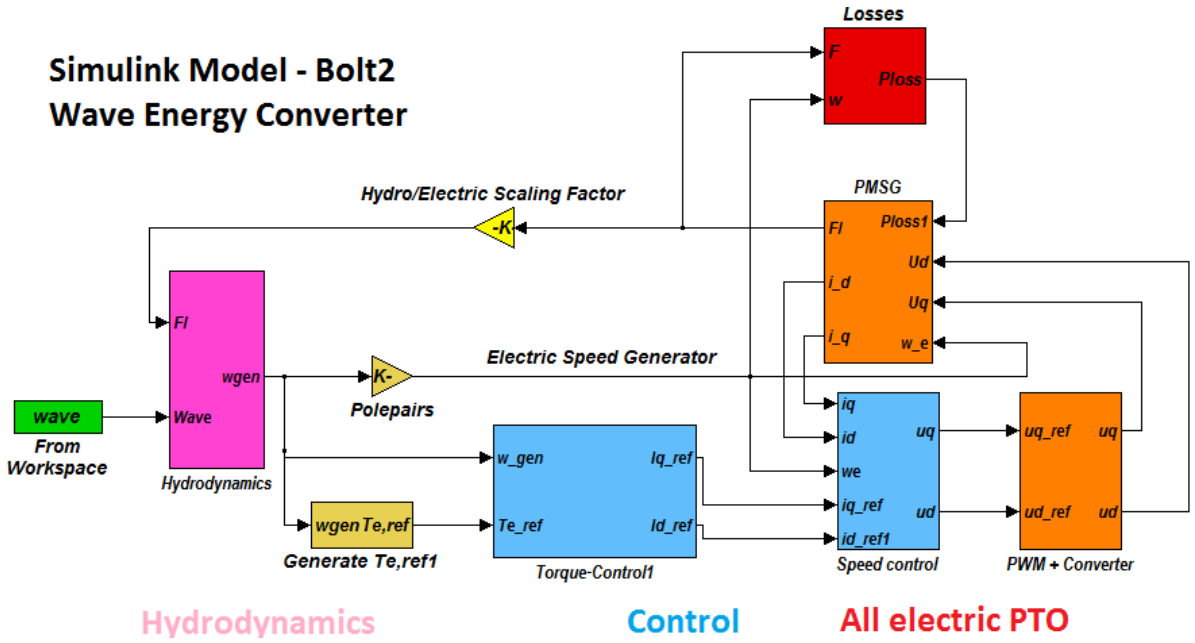

The average extracted mechanical power for this simulation is found to be 1.75 kW, and the generator losses are 0.56 kW. This gives an average efficiency of 66.85% and an electrical output power of 1.17 kW. The low efficiency is typical in low wave states, where the generator has to operate with high torque and low speed.

Figure 12. Plot showing input wave elevation time series. $H_s = 0.5\,m$ and $T_p = 6.5\,s$.

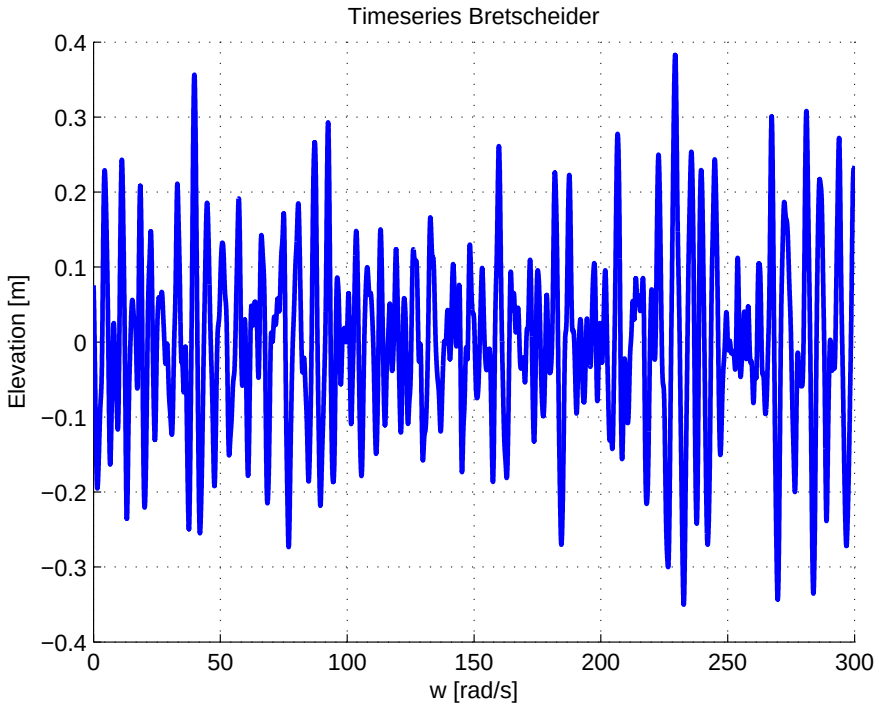

Figure 13. Generator speed for the input wave elevation shown in Figure 12. The red line indicates torque saturation speed; the black line indicates field weakening speed. The system is passively loaded.

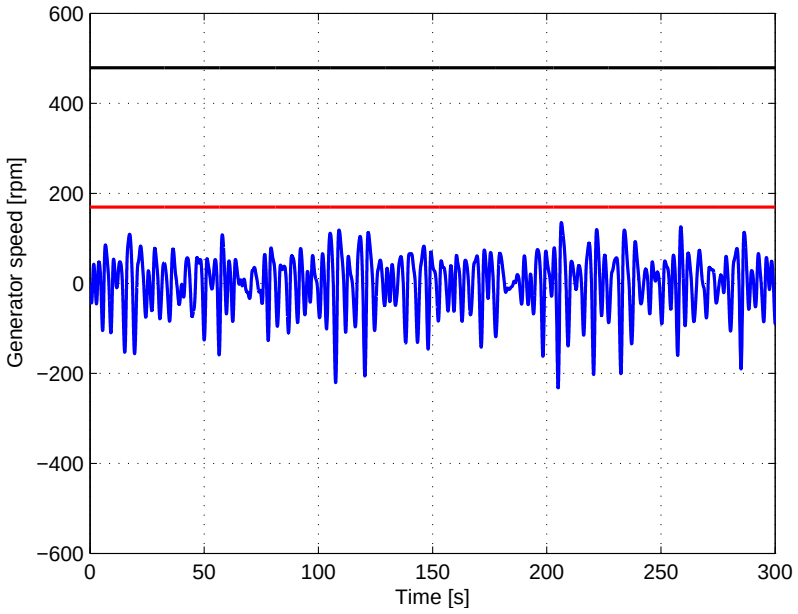

Figure 14. Converter operation for the passively loaded case. (**a**) D-axis current; (**b**) Q-axis current; (**c**) Generator torque.

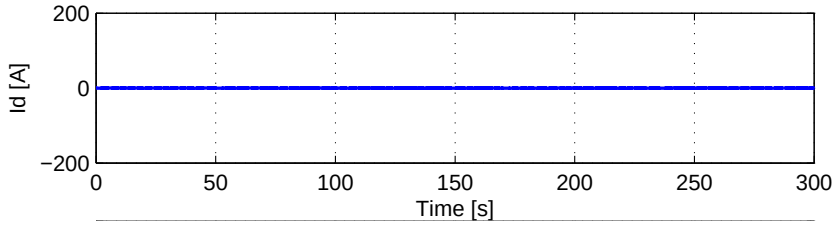

(a)

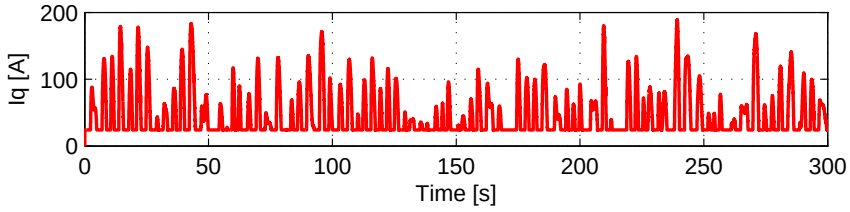

(b)

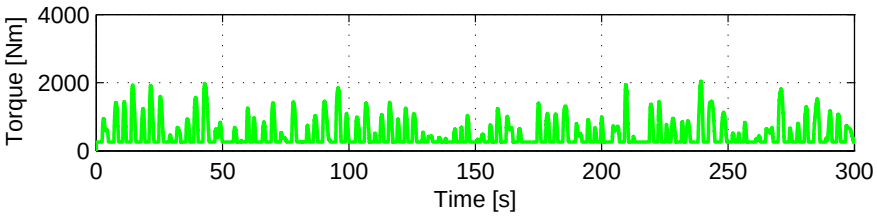

(c)

Figure 15. Generator operation for the passively loaded case. (**a**) Mechanical extracted power; (**b**) Generator losses; (**c**) Electrical output power.

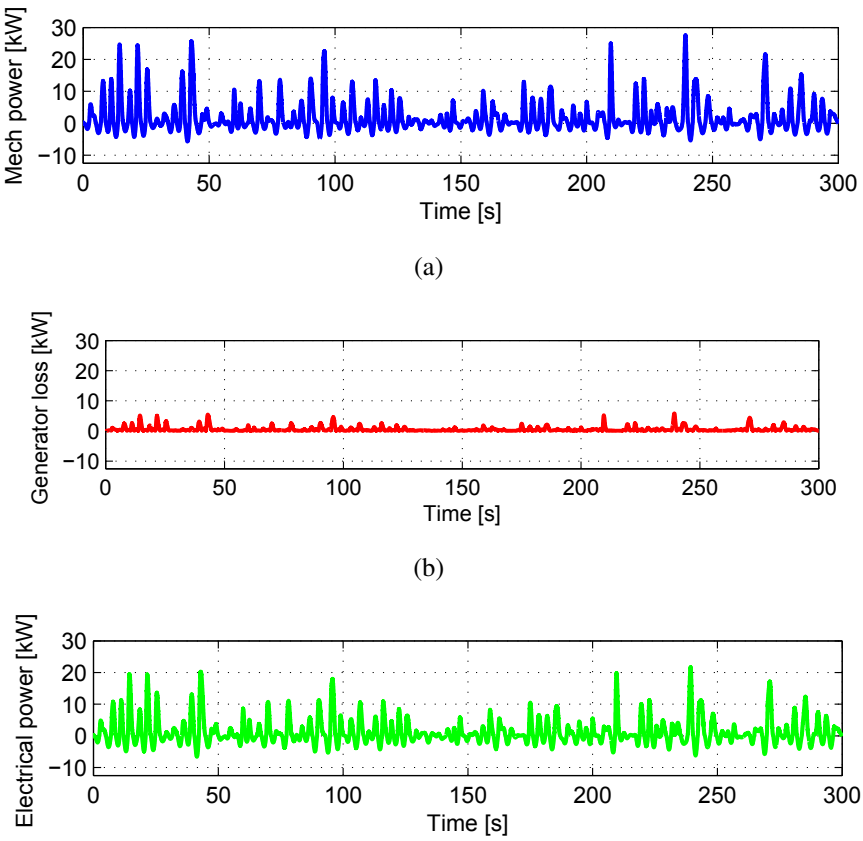

Figure 16. Mechanical extracted power (blue), generator losses (red) and electrical output power (green). The WEC system is passively loaded.

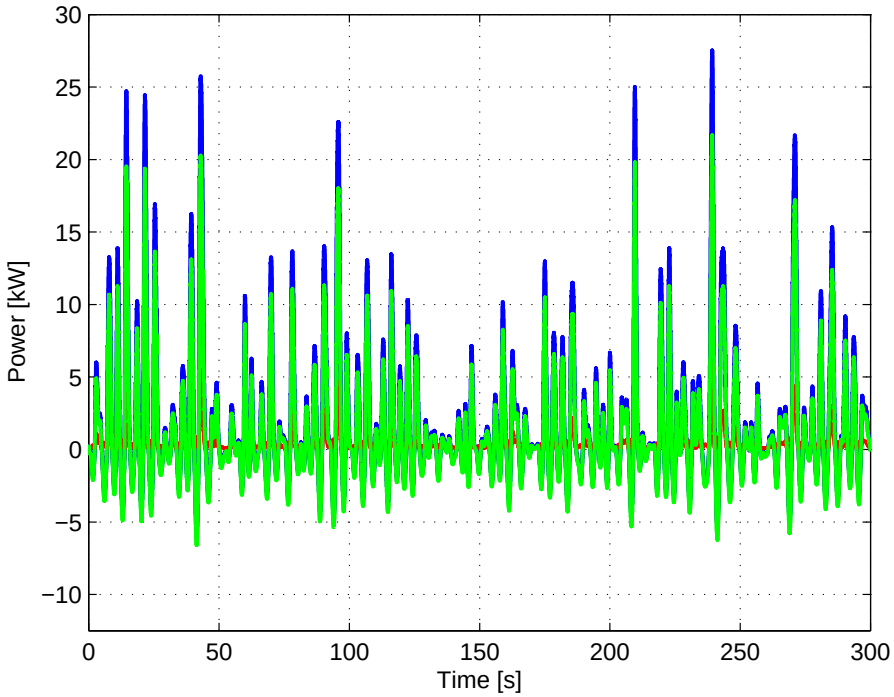

4.2. Simulation Results for a Reactive Controlled System

Now, a wave-to-wire simulation is performed for a similar wave elevation input as seen in Figure 12. The load parameters are tuned according to [10]. This gives a damping, $B_L = 22.1\ kNs/m$, and an added mass, $M_L = 84.4$ tons. The generator speed for such a controlled system can be seen in Figure 17, and as expected, the generator speed is significantly increased when compared to the reference case of passive loading shown in Figure 13. When the generator speed increases above 190.5 rpm, the q-axis current and the torque saturate, as is seen in Figure 18. In Figure 19, the generator speed and torque are plotted in the same normalized figure. In this case, in contrast to the passively loaded system, the torque is not in phase with the generator speed.

Figure 17. Generator speed for the input wave elevation shown in Figure 12. The red line indicates torque saturation speed; the black line indicates field weakening speed. The WEC system is reactively controlled.

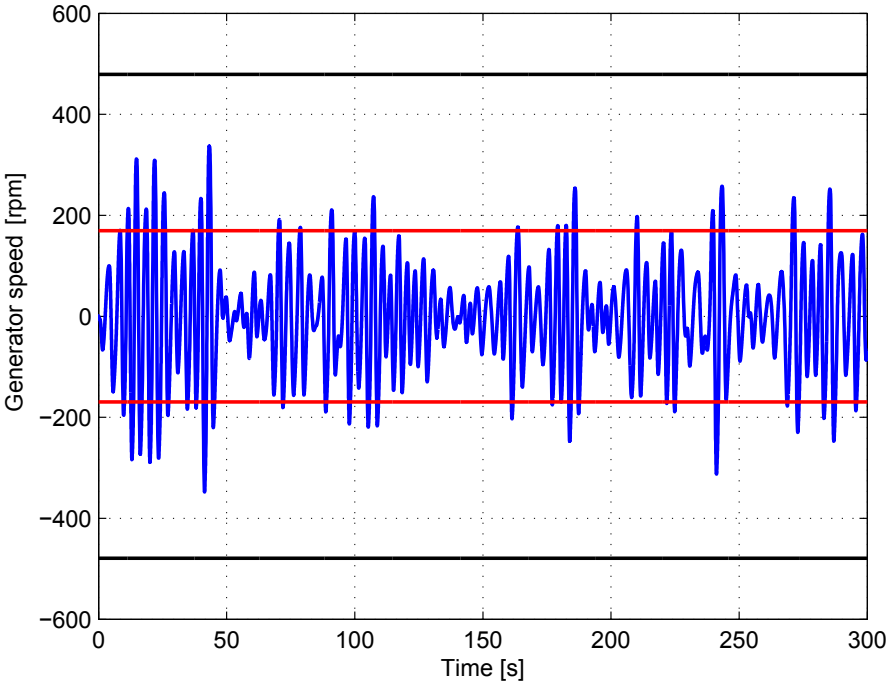

From linear control analysis, it is demonstrated that when a reactive component is added to the applied force, negative power-flow will occur [9]. This can also be understood from the plot of generator speed and force, as seen in Figure 19, where there is a phase difference between these two values. When dealing with the changing direction of the power flow, it is important to evaluate the losses correctly. In the Simulink model, the absolute value of the losses is calculated. The electrical output power is then found by Equation (26). This means that the electrical power will have lower magnitude than the mechanical power in the positive power sequence, but larger magnitude than the mechanical power when the electrical power is negative. The time domain plots for these values are plotted in Figures 20 and 21. Figure 22 shows in a more detailed way how these powers compare to each other between 135 and 145 s.

$$P_{el} = P_{mech} - |P_{loss}| \tag{26}$$

Figure 18. Converter operation for the reactively loaded case. (**a**) D-axis current; (**b**) Q-axis current; (**c**) Generator torque.

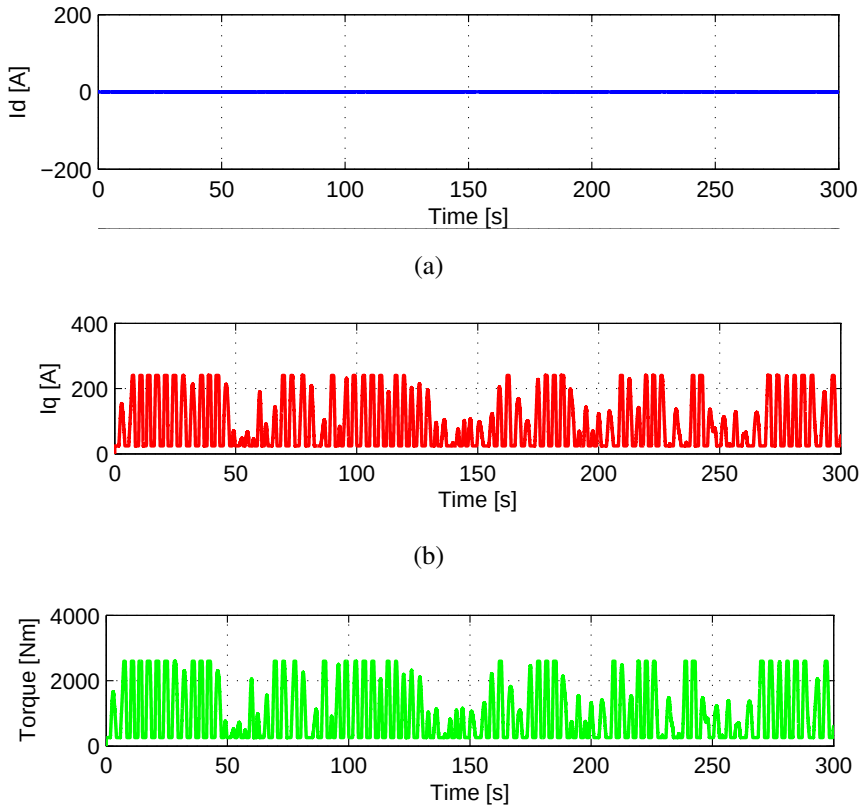

Figure 19. Zoomed-in generator speed (blue) and generator force (red) plotted together and normalized. The WEC system is reactively controlled.

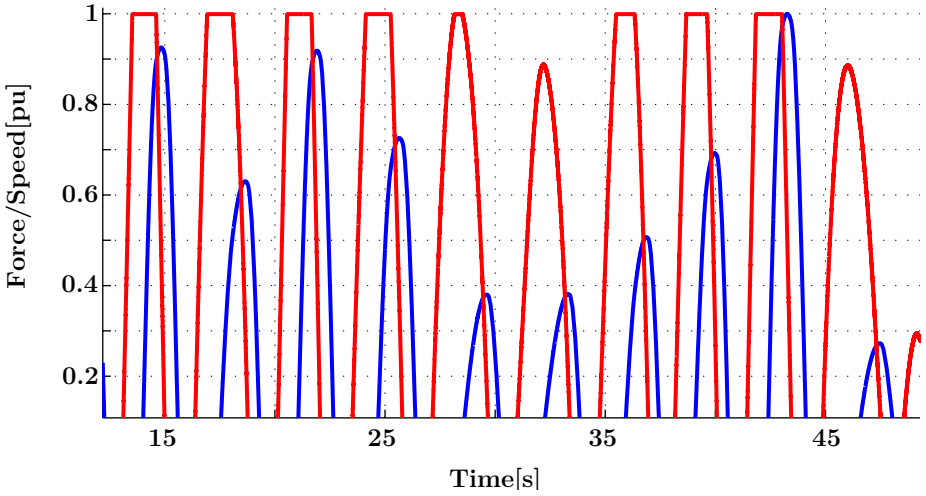

Figure 20. Generator operation for the reactively loaded case. (**a**) Mechanical extracted power; (**b**) Generator losses; (**c**) Electrical output power.

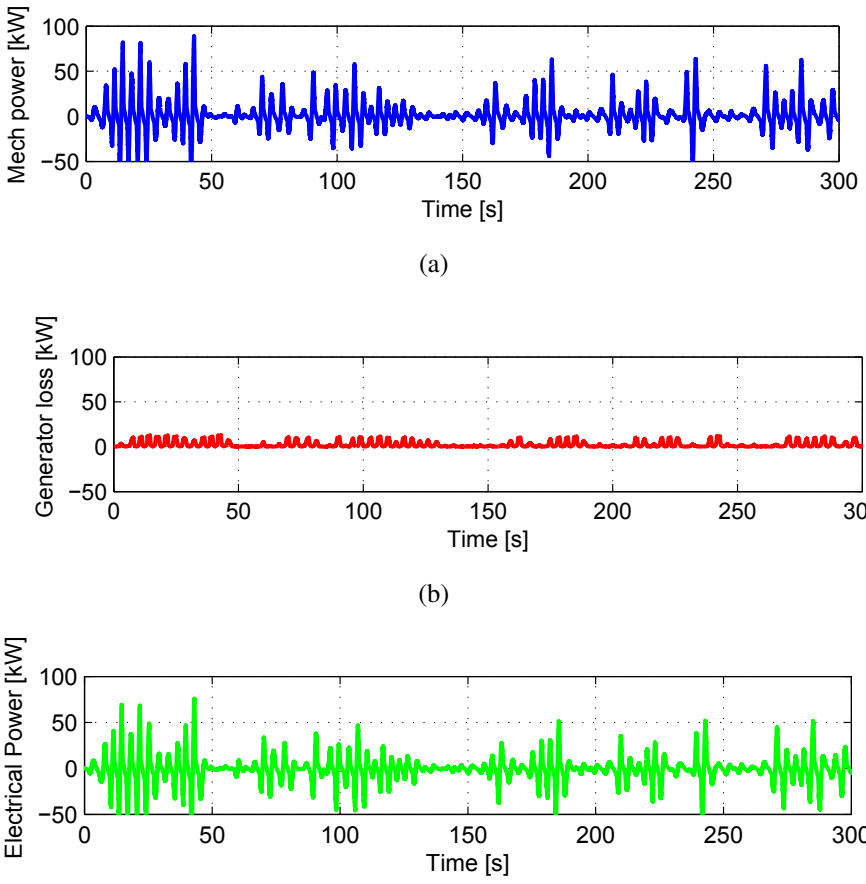

Figure 21. Mechanical extracted power (blue), generator losses (red) and electrical output power (green). The system is reactively controlled.

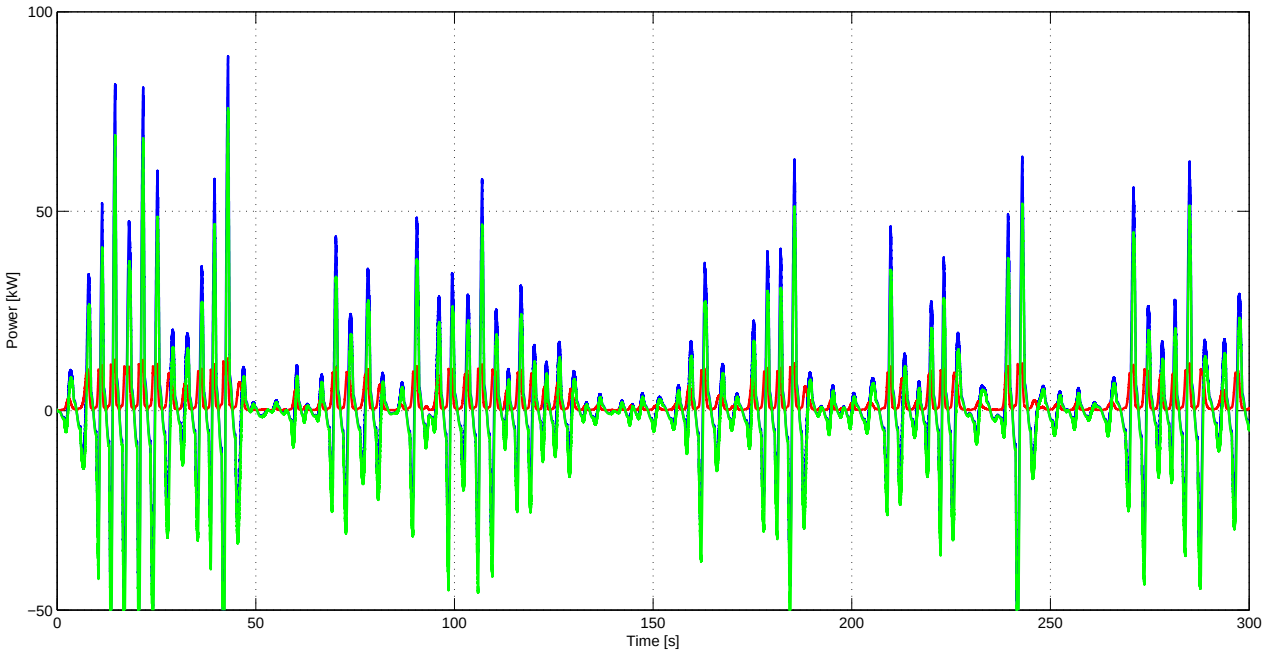

Figure 22. Close-up of mechanical extracted power (blue), generator losses (red) and electrical output power (green). The WEC system is reactively controlled.

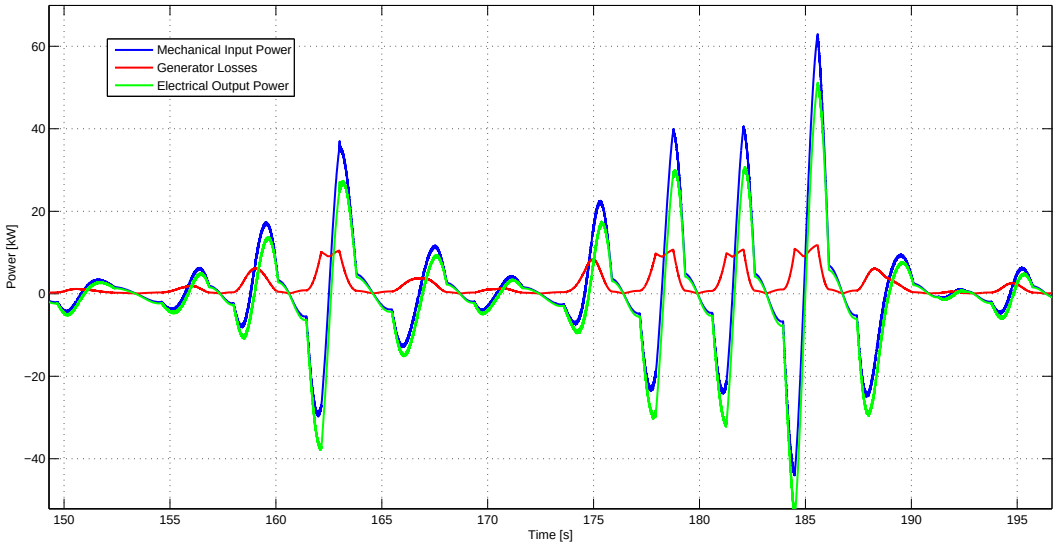

It is important to keep in mind the fact that losses do not behave bidirectionally [20] and that the accumulated average of the losses can become even larger than the average extracted mechanical power. The performed simulation is an example of this; the average extracted mechanical power is 2.57 kW, while the average losses are 2.72 kW. This means that the average output electrical power is −0.15 kW, and the permanent magnet machine consumes more power due to losses than it produces.

4.2.1. Performance of Passive Loading *vs.* Reactive Control

The key result from these simulations is that when taking generator losses into account, the performance of reactive control close to complex conjugate control is not satisfactory [9]. In fact, average delivered power to the grid is negative, meaning that in average power flows from the grid to the ocean. In order to understand why such conditions occur, a few properties about reactive control has to recognized. In order to achieve reactive control, the machinery that supplies the load force not only receives energy, but also has to return some energy. We recognize that by the increased bi-directional power flow, which results in high peaks of received power and lower peaks in returned power. On average, the power is therefore positive. However, as J. Falnes comments in [4], this calls for an energy conversion efficiency preferably close to unity, which is not the case for the Lifesaver generator. The above observations lead to the following conclusions:

- Approximate complex conjugate control leads to increased mechanical power extraction;
- However, the generator efficiency becomes more important, as the bi-directional power peaks both contribute to the average losses;
- As Lifesaver has an average generator efficiency of around 80% in the design wave state and lower efficiency in the lower wave states, the losses can become very large;
- Due to this, approximate complex conjugate control does *not* give maximum electrical power output.

In the following sections, a simulation trial for determining the optimal control parameters for a given sea state will be outlined.

4.3. Maximizing Electrical Output Power-Table for Sub-Optimal Operation Parameters

Optimal control of a wave energy converter is often thought of as the control that gives maximum power extraction or maximum energy absorbed from the sea. However, a practical definition should be the set of control parameters, which gives the maximum electrical power delivered to the grid respecting the physical limits of the WEC device. From now on, the term *optimal control* (or sub-optimal) is used with this definition in mind. It has been shown that linear control theory is not a suitable approach to identify these optimal control parameters for irregular waves. Instead, an analytical solution to the problem can be attempted from the expression of the average extracted power in Equation (27) and the loss approximation expression in Equation (25).

$$P_{opt,el}(R_l, L_L) = max\left(P_M - |P_{loss}|\right) \tag{27}$$

This expression becomes a non-trivial equation to solve as the generator losses is a fourth-order expression dependent on the control parameters, as well as the generator speed. A simplified approach is therefore pursued by running a number of simulations with different load parameters to identify optimal control for each sea state by trial and error. The goal of these simulations is, however, to make a map of optimal control parameters for different sea states.

4.3.1. Example Identification of Optimal Control Parameters for a Low Wave State

The identification of optimal control parameters is performed by scanning step-wise through all values for B_L and M_L. The resulting output is illustrated in Table 3 with some values listed. Notably, the leftmost column corresponds to the purely damped system. The background color in Table 3 illustrates the general trendline for average exported power (red: $<$1 kW, orange: 1–2 kW, yellow: 2–2.5 kW, green: 2.5–2.8 kW, light green: $>$2.8 kW).

The losses are listed in Table 4 with background color levels (red: $>$1.5 kW, orange: 1–1.5 kW, yellow: 0.5–1 kW, green: 0.25–0.5 kW, light green: $<$0.25 kW). Notably, it is observed that maximum generator losses occur when the system is complex conjugate-controlled. This is due to the accumulated average losses of the high bidirectional peaks in power. The losses are lowest for the upper left corner of the table, where the control parameters go towards zero. This is natural as it corresponds to a no-load operation of the generator, and the losses are purely rotational losses.

Combining the two tables, the corresponding electric output table can be seen in Table 5 (red: $<$1 kW, orange: 1–1.25 kW, yellow: 1.25–1.5 kW, green: 1.5–1.6 kW, light green: $>$1.6 kW). As seen from the map, an optimal set of control parameters is identified for this sea state with an added damping, $B_L = 120\,kNs/m$, and an added mass of $M_L = 40$ tons. Notably, the average electric output power is increased by 11.9% compared with the optimal passive load case.

Table 3. Average extracted mechanical power [kW].

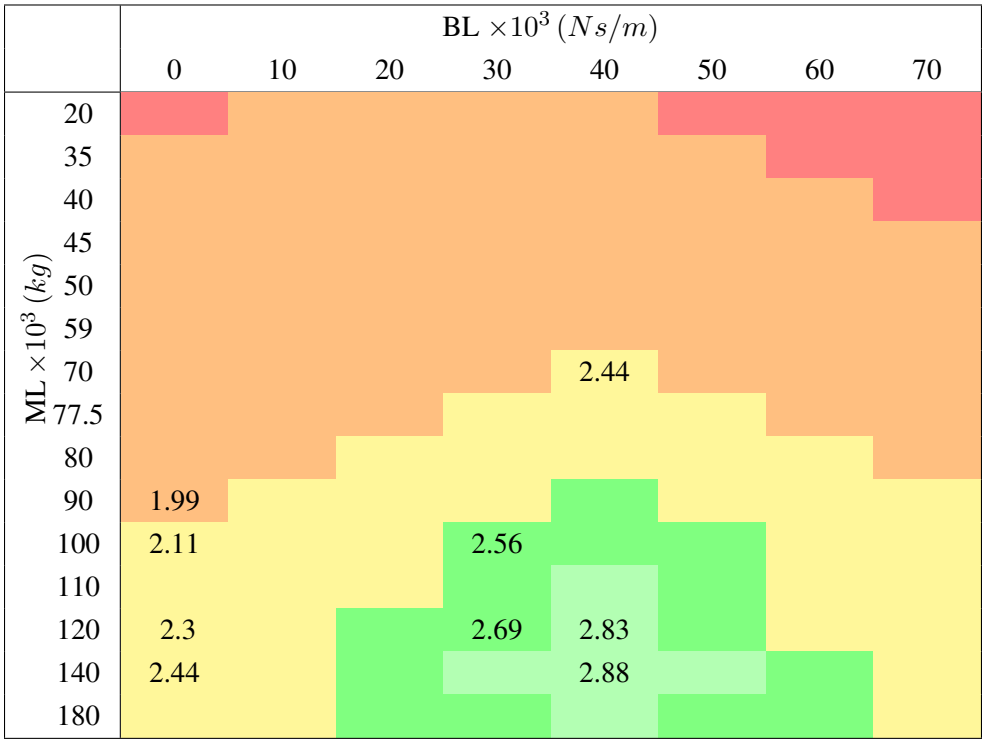

Table 4. Average losses [kW].

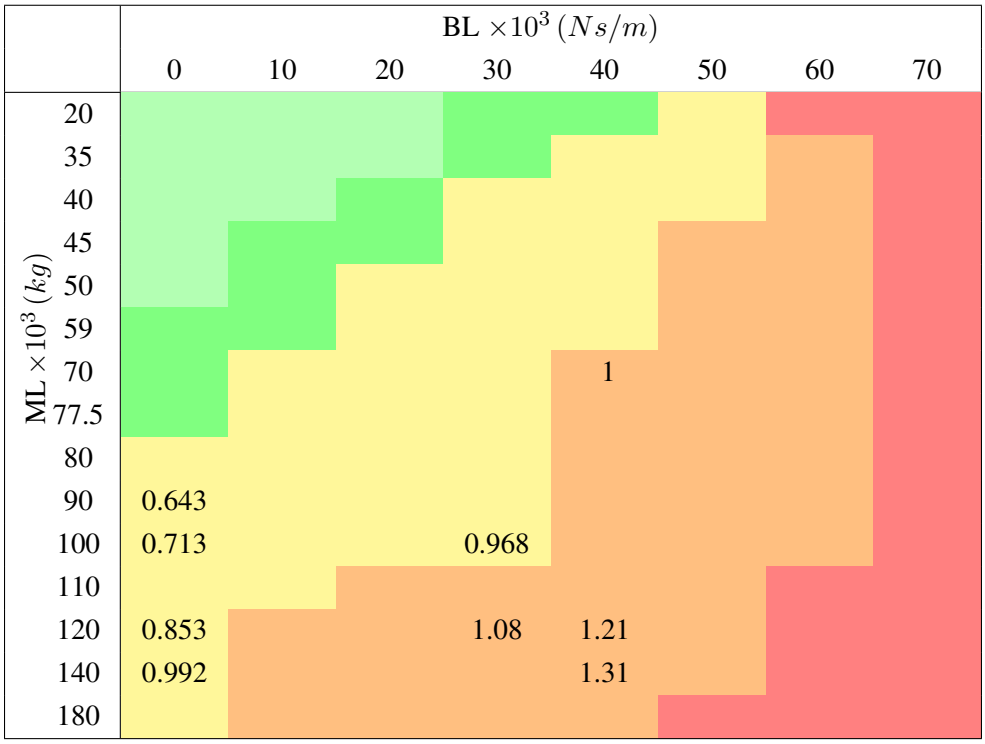

Table 5. Output electric power [kW].

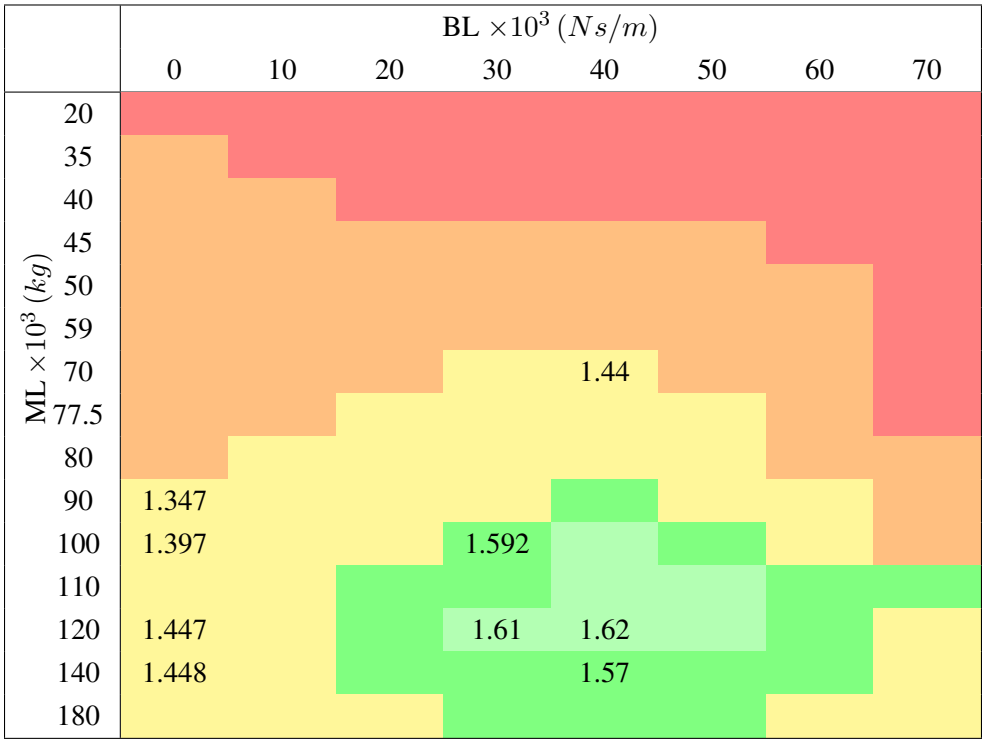

4.3.2. Observations from Mapping of Control Parameters

From a number of simulation results for the different sea states, some general observations can be made from the optimal control parameter mapping.

- Combining the maps of output mechanical power and generator losses, a map of optimal control parameters with respect to electrical output power is made;
- For sea states with low significant wave height, the optimal control parameters have a larger component of added mass and smaller component of added damping;
- For the sea states with low significant height, the average power is increased by a significant factor, *i.e.*, 10% for $H_s = 0.5$;
- When the significant wave height increases, the optimal control parameters shift towards a larger factor of added damping;
- For the sea states with a higher significant wave height, the increase in average power compared with the reference case of passive loading goes towards zero;
- For a sea state with lower peak periods, the optimal control parameters have a larger damping factor;
- For increasing peak periods, the optimal control parameters have larger fraction of added damping. This means that the optimal control moves towards complex conjugate control;
- Average power extraction decreases with increasing peak period of the sea. This is caused by the reduced generator speed and the subsequent generator performance reduction [21,22].

4.4. Energy Calculations-Potential Increase in Annual Energy Production with Optimal Control

By using sea-state statistics, estimations of annual energy production can be made. Previous estimations have been made for the Lifesaver concept [23], and some preliminary investigations have also been performed into a potential increase in annual energy production using reactive control. However, the latter paper does not take into account the generator force limitation or generator losses, and these factors become very significant under reactive control in particular [24]. This means that an investigation into increased energy production using reactive control with generator limitations is a very interesting and novel addition to the former research.

Identification of the optimal control parameters for all sea-states has not been performed. Only selected sea-states were used as a representation of the whole spectra. From the wave scatter diagram in Table 6, one can define the following three sea states:

- $H_s = 0.75\,m$ and $T_p = 4.5\,s$ are the sea states that represents the low energy sea states;
- $H_s = 1.75\,m$ and $T_p = 5.5\,s$ represent the medium energy sea states;
- $H_s = 3.25\,m$ and $T_p = 6.5\,s$ represent the high energy sea states.

Table 6. Wave scatter diagram for Wavehub location. Blue area represents low-energy sea-states, green represents medium energy sea-states and red represents high energy sea-states.

Significant wave height hs [m] \ Wave period Tz [sec]	3,5	4,5	5,5	6,5	7,5	8,5	9,5	10,5	11,5
0,25	26	79	44	18	0	0	0	0	0
0,75	499	832	491	140	18	0	0	0	0
1,25	184	1051	604	307	70	26	9	0	0
1,75	0	587	701	333	149	53	26	0	9
2,25	0	96	534	254	123	44	9	0	0
2,75	0	0	237	228	105	26	9	9	0
3,25	0	0	26	175	123	44	9	0	0
3,75	0	0	0	79	96	35	18	0	0
4,25	0	0	0	9	44	26	9	9	0
4,75	0	0	0	0	26	18	9	0	0
5,25	0	0	0	0	18	26	18	0	0
5,75	0	0	0	0	0	18	9	0	0
6,25	0	0	0	0	0	9	0	0	0

Defining the different sea states in Table 6 as one of these three and summing the total annual hours results in Table 7. Using the similar approach, as seen in the previous section, Table 7 lists the average power extraction for each of the three defined sea states for both optimal passive loading and optimal control parameters from an electrical output perspective. The results show that an annual energy production increase of 1% is a fair estimation for Lifesaver if optimal reactive control is implemented.

Table 7. Power and energy calculations for the representative sea states.

	Low energy	**Medium energy**	**High energy**	**Total**
Hours per wave state	2182	4370	2468	8760
Av. Pow. Pass. (kW)	6.70	19.04	31.40	-
Av. Pow. Opt. (kW)	7.02	19.24	31.47	-
Diff (%)	4.78	1.4	0.22	-
Ener. Pass. (MWh)	14.62	83.22	77.53	175.37
Ener. Opt. (MWh)	15.32	84.10	77.70	177.12
Difference (%)	4.78	1.40	0.22	1.0

5. Discussion

The main motivation of this article was to develop a full wave-to-wire model of the Lifesaver WEC and to use this model to investigate how to control the device in order to extract maximum power under given physical constraints. Based on this, the key observations are summarized below:

- A full wave-to-wire model of Lifesaver point absorber with all-electric power take off system has been made in Matlab and Simulink;
- The main characteristics of the Lifesaver generator and power take off system have been modeled using classical representation of a Permanent Magnet Synchronous Machine complete with field weakening operation and a simplified model of the inverter and DC-link;
- A control method has been demonstrated that enforces the force, voltages and currents within the different rating constraints of the power take-off system, even for the sea states with high significant wave height;
- Wave-to-wire simulations show that Lifesaver has limited potential for increased power extraction using reactive control, due to the force and efficiency limitations of the generator; Analysis shows that the if the device is optimally controlled, only a 1% increase in annual energy production can be expected compared to the reference case of passive loading.

5.1. Aspects of Practical Implementation in Lifesaver

As Lifesaver is currently deployed in the ocean for an extensive testing period, the results reported in this article can also be experimentally verified. There is naturally some degree of uncertainty regarding how realistic the developed model is of the real-life Lifesaver WEC. This is especially due to the following factors:

- Hydrodynamic model of Lifesaver is not completely accurate;
- The validity and accuracy of the simplified PMSM model used;
- The damping coefficients used by Lifesaver in the sea are not the same found to give optimal power extraction in the model.

Still, it is interesting to investigate the effect of reactive control on the physical device. A control strategy can be suggested for a preliminary test of Lifesaver's response to reactive control based on the

observations done in this model. As a rule of thumb, the results in this investigation finds that optimal control of Lifesaver occurs with an added mass of approximately 10% of the added damping. However, undertaking such an investigation might not be desirable if the theoretical maximum annual increase in energy is only 1%. It is therefore important to analyze the initial test in detail in order to evaluate if the limited potential described in this article could be valid also in reality.

5.2. Implications for a Generic WEC

Several of the observations in this article could be very useful for a generic point absorber and can thus be implemented in the planning and research of future wave energy devices. Primarily, this is true regarding how to develop a wave-to-wire model based on hydrodynamic measurement data of the device and on the electric power take-off ratings. Perhaps the most interesting point is that such a wave-to-wire model can be used to investigate control techniques and decide on favorable power electronics and generator ratings at an early stage of the concept development. In order to do this, one would need hydrodynamic parameters, like the excitation force coefficient, radiation resistance and the mass of the device for a range of different frequencies. These can either be obtained by model testing of a prototype or by some software analysis (using WAMITand ACQUA).

6. Conclusions

Wave-to-wire simulations show that implementing reactive control with load parameters close to approximate conjugate control does not give increased electrical output power. This is because the high peak-average ratio of approximate complex conjugate control gives large accumulated average losses, and in the extreme examples these, losses can be larger than the average extracted mechanical power, meaning electric power is, on average, extracted from the grid. An intermediate control strategy based on a smaller component of added mass is found to be the optimal control strategy from an electrical output power point of view, and the optimal control parameters for a set of representative sea states is identified. Annual energy estimations are performed based on a set of representative sea states. Compared to the reference case of passive loading, the optimally controlled Lifesaver shows an annual increase in energy production of 1%. This indicates that Lifesaver has low potential for increased power extraction using reactive control, and it is recognized that this is due to the non-negative minimum force restriction of the power take-off system and the limited efficiency of the generator. These results should be verified by practical implementation on Lifesaver, but must be weighed against the cost of updating the control software, as the expected production gain is marginal.

The limited effect of reactive control on Lifesaver has been demonstrated through a series of wave-to-wire simulations. This analysis of the power take-off capability of the Lifesaver WEC is nonetheless valuable, especially for future development of point absorber wave energy devices. In addition to demonstrating the development of a wave-to-wire model of a WEC, perhaps the most important contribution of this investigation is in highlighting some of the major advantages, properties and drawbacks of the PTO capabilities of all electric direct-driven point absorbers.

Acknowledgments

We would like to thank Fred. Olsen for funding the Wave Energy Project. The work of Elisabetta Tedeschi was supported by a Marie Curie Intra-European Fellowship within the 7th European Community Framework Programme (FP7-PEOPLE-2010-IEF n.272571). The work of Jonas Sjolte was supported by the Norwegian Research Council under the program *NæringsPhd*.

References

1. Thorpe, T. *2010 Survey of Energy Resources*; Technical Report for World Energy Council: London, UK, 2010.
2. International Energy Agency (IEA). *Electricity in the World*; Technical Report; IEA: Paris, France, 2008.
3. Wave Hub. Available online: http://www.wavehub.co.uk (accessed on 12 July 2013).
4. Falnes, J. *Ocean Waves and Oscillating Systems, Linear Interaction Including Wave-Energy Extraction*; Cambridge University Press: Cambridge, UK, 2002.
5. Falnes, J. *Principles for Capturie of Energy from Ocean Waves: Phase Control and Optimum Oscillation*; Technical Report for Norwegian University of Science and Technology: Trondheim, Norway, 1997. Available online: http://folk.ntnu.no/falnes/w_e/index.html (accessed on 12 July 2013).
6. Falnes, J.; Hals, J. Heaving buoys, point absorbers and arrays. *Philos. Trans. R. Soc. A Math. Phys. Eng. Sci.* **2012**, *370*, 246–277.
7. Falnes, J.; Lillebrekken, P.M. Budal's Latching-Controlled-Buoy Type Wave-Power Plant. In Proceedings of the 5th European Wave Energy Conference, Cork, Ireland, 17–20 September 2003.
8. Hals, J. Modelling and Phase Control of Wave-Energy Converters. Ph.D. Thesis, Norwegian University of Science and Technology, Trondheim, Norway, 2010.
9. Tedeschi, E.; Molinas, M. Tunable control strategy for wave energy converters with limited power takeoff rating. *IEEE Trans. Ind. Electron.* **2012**, *59*, 3838–3846.
10. Sandvik, C.; Molinas, M.; Sjolte, J. Time Domain Modelling of the Wave-to-Wire Energy Convert Bolt. In Proceedings of the 7th International Conference and Exhibition on Ecological Vehicles and Renewable Energies, Monte Carlo, Monaco, 22–25 March 2012.
11. Mitchell, W.H. Sea spectra revisited. *Mar. Technol.* **1999**, *4*, 211–227.
12. Dean, R.; Dalrymple, R. *Water Wave Mechanics for Engineers and Scientists*; Prentice Hall: Upper Saddle River, NJ, USA, 1984.
13. Newman, J. *Marine Hydrodynamics*; Mit Press: Cambridge, MA, USA, 1977.
14. Cummins, W.E. *The Impulse Response Functions and Ship Motions*; Department of the Navy, David Taylor Model Basin: Bethesda, MD, USA, 1962.
15. Taghipour, R.; Perez, T.; Moan, T. Hybrid frequencytime domain models for dynamic response analysis of marine structures. *Ocean Eng.* **2008**, *35*, 685–705.
16. Kung, S. A New Identification and Model Reduction Algorithm via Singular Value Decompositions. In Proceedings of the 12th Aslilomar Conference on Circuits, Systems and Computers, Pacific Grove, CA, USA, 6–8 November 1978; pp. 705–714.

17. Mohan, N. *Advanced Electric Drives Analysis, Control and Modeling Using Simulink*; Minnesota Power Electronics Research & Education (MNPERE): Minneapolis MN, USA, 2001.
18. Umland, J.; Safiuddin, M. Magnitude and Symmetric Optimum Criterion for the Design of Linear Control Systems—What Is It and Does It Compare with the others? In Proceedings of the IEEE Industry Applications Society Annual Meeting, Salt Lake City, UT, USA, 2–7 October 1988; pp. 1796–1802.
19. Pan, C.T.; Liaw, J.H. A robust field-weakening control strategy for surface-mounted permanent-magnet motor drives. *IEEE Trans. Energy Conver.* **2005**, *20*, 701–709.
20. Tedeschi, E.; Molinas, M.; Carraro, M.; Mattavelli, P. Analysis of Power Extraction from Irregular Waves by All-Electric Power Take off. In Proceedings of the IEEE Energy Conversion Congress and Exposition (ECCE), Phoenix, AZ, USA, 12–16 September 2010; pp. 2370–2377.
21. Sjolte, J.; Bjerke, I.; Hjetland, E.; Tjensvoll, G. All-Electric Wave Energy Power Take off Generator Optimized by High Overspeed. In Proceedings of the Submitted to the European Wave and Tidal Energy Conference (EWTEC11), Southampton, UK, 5–9 September 2011.
22. Molinas, M.; Skjervheim, O.; Sørby, B.; Andreasen, P.; Lundberg, S.; Undeland, T. Power Smoothing by Aggregation of Wave Energy Converters for Minimizing Electrical Energy Storage Requirements. In Proceedings of the Submitted to the European Wave and Tidal Energy Conference (EWTEC07), Porto, Portugal, 11–13 September 2007.
23. Sjolte, J.; Tjensvoll, G.; Molinas, M. All-Electric Wave Energy Converter Array with Energy Storage and Reactive Power Compensation for Improved Power Quality. In Proceedings of the IEEE Energy Conversion Congress and Exposition (ECCE), Raleigh, NC, USA, 15–20 September 2012; pp. 954–961.
24. Tedeschi, E.; Molinas, M. Impact of Control Strategies on the Rating of Electric Power Take off for Wave Energy Conversion. In Proceedings of the IEEE International Symposium on Industrial Electronics, Bari, Italy, 4–7 July 2010; pp. 2406–2411.